Edge passivation of shingled poly-Si/SiOx passivated contacts solar cells

Franck Dhainaut, Raoul Dabadie, Benoit Martel, Thibaut Desrues, Mickaël Albaric, Olivier Palais, Sébastien Dubois, Samuel Harrison

EPJ Photovoltaics **14**, 22 (2023)

https://doi.org/10.1051/epjpv/2023013

Available online at:
www.epj-pv.org

REGULAR ARTICLE OPEN ACCESS

Edge passivation of shingled poly-Si/SiO_x passivated contacts solar cells

Franck Dhainaut[1,2,*], Raoul Dabadie[1], Benoit Martel[1], Thibaut Desrues[1], Mickaël Albaric[1], Olivier Palais[2], Sébastien Dubois[1], and Samuel Harrison[1]

[1] Univ. Grenoble Alpes, CEA, Liten, Campus Ines, 73375 Le Bourget du Lac, France
[2] Aix Marseille Université, Université de Toulon, CNRS, IM2NP, Marseille, France

Received: 14 March 2023 / Received in final form: 11 May 2023 / Accepted: 2 June 2023

Abstract. This work aims at the full recovery of efficiency losses induced by shingling double-side poly-Si/SiO_x passivated contacts crystalline silicon solar cells. It focuses on thermally-activated Aluminium Oxide (AlO_x) layers elaborated by thermal Atomic Layer Deposition (ALD) to passivate the edges of shingled cells cut by using the innovative "45° tilt squaring approach". The whole procedure featuring high-temperature AlO_x annealing led to very low cut-related performance losses. Indeed, the efficiency and FF of the passivated shingled cells surpassed the values obtained for the as-cut shingles by $0.5\%_{abs}$ and $2.6\%_{abs}$, respectively. Approaches for further improvements are also discussed, particularly to overcome the short-circuit current density decrease observed for passivated shingles.

Keywords: Shingle solar cell / passivated contacts / edge passivation / AlO_x / high temperature

1 Introduction

Already produced by several manufacturers, the so-called "shingle" modules are expected to represent 8% of the world market share within a decade [1]. This interconnection method presents several benefits such as a reinforced shading resilience [2], an improved reliability [3] as well as superior aesthetics. The shingle architecture also allows an increased active module area, obtained from the in-between cells space and metallization shading reductions [3]. Its main strength lies yet in the ability to further reduce the power dissipation due to resistive losses in the interconnections (in comparison with large-scale manufactured half-cell modules) [4], which leads to a higher Fill Factor (FF). As a result of the two latter aspects, such devices using cells of reduced size could allow an output power increase by more than $10\%_{rel}$ compared to conventional interconnections according numerical simulations [5,6]. However, in practice, edge-related harmful effects limit this potential gain, especially for solar cells exhibiting high Open Circuit Voltage (V_{OC}) values [7,8], such as silicon heterojunction or poly-Si based passivated contacts approaches. In addition, as the perimeter-over-area ratio increases, the cell's performance is even more affected by its edges [9].

As the mono-crystalline silicon (c-Si) wafer size in the market tends to keep increasing, with the current standard M10 format shifting to G12 format, it is more interesting for costs reasons to process the cells on full wafers and then cut the hosts cells into subcells rather than processing small wafers. However, this cutting action creates new unpassivated bare edges, more defective and therefore more recombination-active than native edges (edges inherited from the original manufacture of the cell), which further degrades the cell's performances. Therefore, using the shingling technology on silicon heterojunction solar cell leads to an overall efficiency loss in the order of $1\%_{abs}$ [10]. In a nutshell, the shingle interconnection is a very promising concept that could significantly reduce the cell-to-module losses, provided that a solution to the edge passivation hurdle is implemented.

Several studies investigated this topic and demonstrated the feasibility of an effective edge passivation. For example, the creation of an emitter window along the cell's border, interrupting this highly conductive path for carriers to the edges, has been shown to be beneficial [11]. Other approaches can take advantage of one or both of the so-called *chemical passivation* and *field effect passivation* (FEP) mechanisms. The first relies on the neutralization of recombination centres, in particular silicon dangling-bonds, and the latter limits the concentration of one kind of carriers (i.e. electrons or holes) at the vicinity of the edge. A recent study based on the FEP mechanism showed notable results with a spraying

* e-mail: franck.dhainaut@cea.fr

process of organic solution (Nafion) during the cutting process [12]. Dielectric layers, in particular Aluminium Oxide (AlO_x), are interesting for both passivation mechanisms. The interface defect density can be reduced thanks to a hydrogen diffusion toward the Si/SiO_x interface of the SiO_x interlayer [13,14]. Furthermore, a FEP occurs due to negative fixed charges in the AlO_x layer, repelling electrons from the edge. The FEP is tremendously enhanced after a post-deposition thermal treatment above 220 °C [15], and become strong enough to offer high surface passivation levels on both n- and p-type crystalline silicon (c-Si) [16,17]. Atomic Layer Deposition (ALD) appears to be the most indicated way to elaborate AlO_x in order to address the purpose of edge passivation, as this deposition process features an excellent conformity. AlO_x deposition conditions, such as chemical precursors and temperature, as well as thickness and annealing temperature, affect the silicon surface passivation level [18–21]. The ALD process suffers from a low deposition rate, which currently limits its interest for industrial applications. However, the evolution of ALD processes, such as spatial ALD [22] or plasma enhanced ALD [23], allows higher throughput to be achieved. Pseudo Fill-Factor (p-FF) cutting-related losses recovery up to $50\%_{rel}$ and $58\%_{rel}$ for bifacial PERC [24] and silicon heterojunction solar cells [25], respectively, have been demonstrated with the application of the AlO_x-ALD edge passivation approach with a low-temperature (<225 °C) post-deposition thermal treatment. Furthermore, a recent study has demonstrated the ability of this approach to achieve larger p-FF values for poly-Si/SiO_x passivated contact (TOPCon) shingles compared to uncut solar cells [26], still using low-temperature annealing (250 °C). This temperature-stable architecture [27], in comparison with heterojunction devices featuring hydrogenated amorphous silicon layers, could benefit from a better activation of the AlO_x layer due to its ability to withstand higher thermal budgets. This is what is investigated here. More precisely, this work describes the application of an ALD-AlO_x edge passivation protocol on advanced double-side poly-Si/SiO_x passivated contacts solar cells. Interestingly, this cell architecture can withstand thermal budgets up to 350–400 °C [28], allowing to reach optimized AlO_x passivation properties.

2 Experimental details

Laser-induced damages to the cut edge resulting from the conventional Laser-Scribing-Mechanical-Cleaving method are known to limit the AlO_x passivation potential, when compared to edge quality obtained with alternative Thermal Laser Separation [20]. In this study, we preferred a laser-free method relying on fully mechanical cleave. Thus, we used 45° tilted silicon bricks for the wafer production with standard squaring and wafering process implementing diamond wire sawing. This kind of substrates presents the (110) preferential crystalline cleaving planes parallel to the edges [25]. Also, the resulting mechanically cleaved edges feature a smooth surface roughness [29]. We used 180 µm-thick, n-type Cz wafers of M2 size (156.75 mm × 156.75 mm), with a resistivity in the range of 1.3 Ω cm to 1.4 Ω cm. Both sides of the wafers

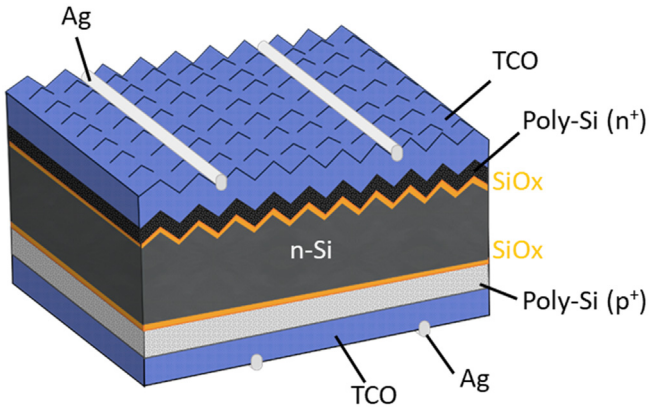

Fig. 1. Double side poly-Si/SiO_x passivated contacts solar cell.

were etched about 10 µm with KOH solution to remove saw-damages, and one side went under (111) pyramidal texturing step.

The cells prepared from these wafers feature ultra-thin poly-Si/SiO_x passivated contacts on both surfaces and a rear emitter configuration, as presented in Figure 1. Tunnel-SiO_x layers are thermally grown in the Low-Pressure Chemical Vapor Deposition (LPCVD) equipment used to subsequently elaborate the 15 nm-thin intrinsic polysilicon layers. Plasma Immersion Ion Implantation (PIII) with B_2H_6 and PH_3 precursors is then used for the boron (rear surface) and phosphorus (front surface) doping of the intrinsic polysilicon layers. Dopants are activated during an 875 °C furnace anneal and their concentration reach more than 1×10^{20} at.cm^{-3}. The samples are then treated in a hydrofluoric acid (HF) solution. For contacting the 15 nm-thin poly-Si layers while maintaining high surface passivation levels, in-situ-hydrogenated indium-tin-oxide layers, acting as TCO (Transparent Conductive Oxide), are deposited by Physical Vapor Deposition (PVD) on the poly-Si layers. The obtained thicknesses are about 70 nm and 100 nm at the front and the rear side, respectively. Low-temperature silver pastes are screen-printed by applying a pattern adapted to the production of six 156.75 mm × 26 mm shingles per host cell. A post-metallization curing annealing step is then conducted in an oven at 350 °C. This fabrication process is shown in Figure 2.

In order to obtain an AlO_x layer with a thickness of about 15 nm, we run 150 thermal ALD cycles in a conventional batch TF500 BENEQ equipment. The process is carried out at less than 1 mbar and 100 °C with TriMethylAluminium and water vapour as gaseous precursor couple. The pulses/purges cycle time is about 10 s. After the dielectric layer deposition, passivated samples undergo a thermal treatment at 400 °C for 3 min in an oven under N_2 gas flow to optimize the AlO_x layer passivation properties.

We compared the performances of three groups of at least three samples: (i) as-cut shingles (S1), without AlO_x and without the thermal treatment; (ii) edge-passivated shingles (S2), with an AlO_x layer covering the edges and

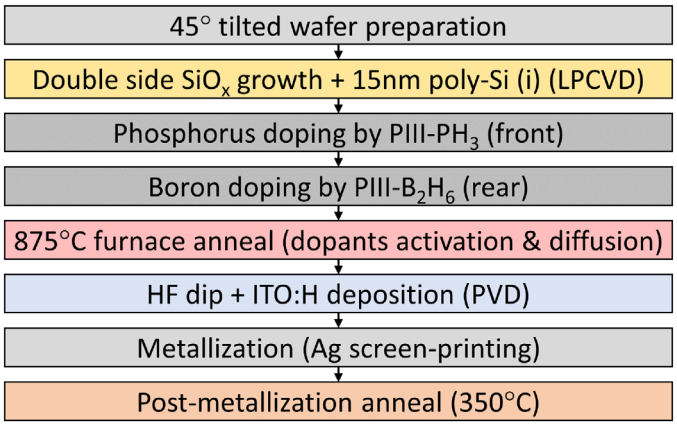

Fig. 2. Fabrication process flow of the double side Poly-Si/SiO_x passivated contacts solar cell.

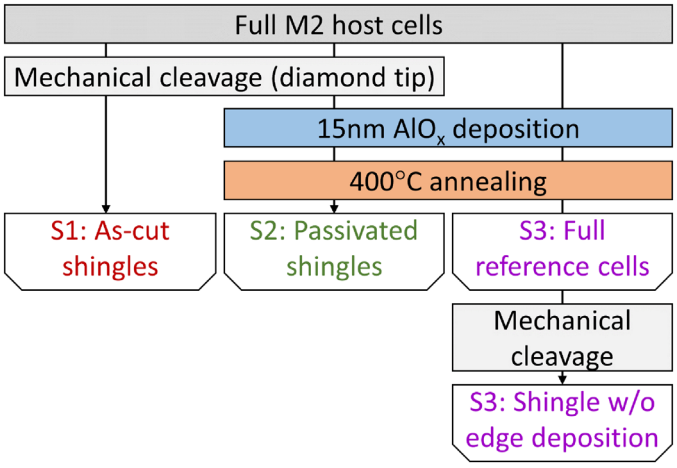

Fig. 3. Design of experiment.

both the front and rear surfaces followed by the 400 °C annealing step; and (iii) full M2 uncut cells (S3) as references of the passivation protocol's impact, featuring the same AlO_x layer on both front and rear sides as well as the annealing step. Host cells cleave to obtain shingles is done by initiating a crack with a diamond tip, followed by a bending stress. The design of experiment is presented in Figure 3.

We conducted current–voltage (IV) measurements under standard AM1.5 spectra to monitor the evolution of each group and assess the effect of both the separation and passivation protocol on the shingled cells performances. The Pasan Spot^{LIGHT} HighCap equipment used is designed for M2 format cell with a non-uniformity of irradiance specified of less than 1%. Shingles were reassembled like a host cell in the equipment for the IV measurements after separation, meaning that 6 cut cells (i.e. shingles) were measured together. However, the IV measurement of reassembled shingles in the automated industrial equipment is tricky because they shift during movements on the belts. In order to avoid displacement of the shingles, we fixed them together with small pieces of polyamide adhesive positioned on the backside. Also, to limit any degradation of the samples due to this handling, no intermediate IV measurements were conducted on the split S2 between cleave and the post-deposition annealing step. Nevertheless, SunsV_{OC} measurements were done at each stage of the separation and passivation sequences of the S2 group. Measurements were conducted on three points for each shingle, before and after their separation, as presented in the Figure 4a.

To assess the specific edge passivation of the cut edges, we applied photoluminescence (PL) imaging [30] on S2 shingles along the whole passivation protocol. We used a high magnification lens on a PL equipment from BTI manufacturer (LIS-R2 model). To obtain a qualitative characterization procedure, a mean edge PL profile is extracted on ImageJ software [31]. Since the profile is obtained by averaging the values of the columns of pixels on the 3 mm − long studied area (annotated in Fig. 5a), a preliminary image processing, consisting of a simple rotation, is necessary to adjust the verticality of the edge in order to ensure the reliability of the obtained profile.

Light Beam Induced Current (LBIC) mappings were finally been conducted on S2 shingles. The results were compared with mappings conducted on shingles prepared from the S3 M2 cells (referred to as S3 shingles). S3 shingles were obtained by the same cleaving protocol realized after AlO_x deposition and annealing of the host M2 cell. Both S2 and S3 shingles have AlO_x layer on the front and rear sides, but only S2 shingles have their edge covered by AlO_x and therefore passivated. The LBIC characterization is obtained with a Semilab equipment using a laser diode with a wavelength of 852 nm scanning the front side. The data exploitation is analogous to the PL method, i.e. a mean signal profile is extracted on Semilab's Wintau software and plotted in a graph. As the mechanical cleaving step is not exactly the same for each shingle, the edge-to-metal distance is not identical. Thus, in order to be able to compare the two shingle edges correctly without the influence of the metal, the LBIC and PL data processing were carried out by fragmenting the area over which the signal is averaged over 1 mm-large areas strictly between the fingers (annotated in Fig. 7a).

3 Results and discussion

p-FF results of S2 and S3 groups are presented in Figure 4b. We can see an important decrease of about $1.9\%_{abs}$ for the p-FF of the S2 group cells after cleave. This decrease reaches $2.3\%_{abs}$ for S1 group (not showed). The mechanical cleavage method performed manually could explain this difference, as a variable amount of damage related to crystal disorientation could be induced at the edges [32]. The V_{OC} results are not shown in the graph, but we report similar decrease for both S1 and S2 groups after shingling.

A noticeable p-FF increase of $0.7\%_{abs}$ in mean is observed directly after the AlO_x layer deposition on S2 shingles. Such a favourable effect of this non-annealed AlO_x layer has not been observed in the study of Martel et al. on silicon heterojunction solar cells [25], in spite of identical deposition conditions. However, Baliozian et al. [24] as well

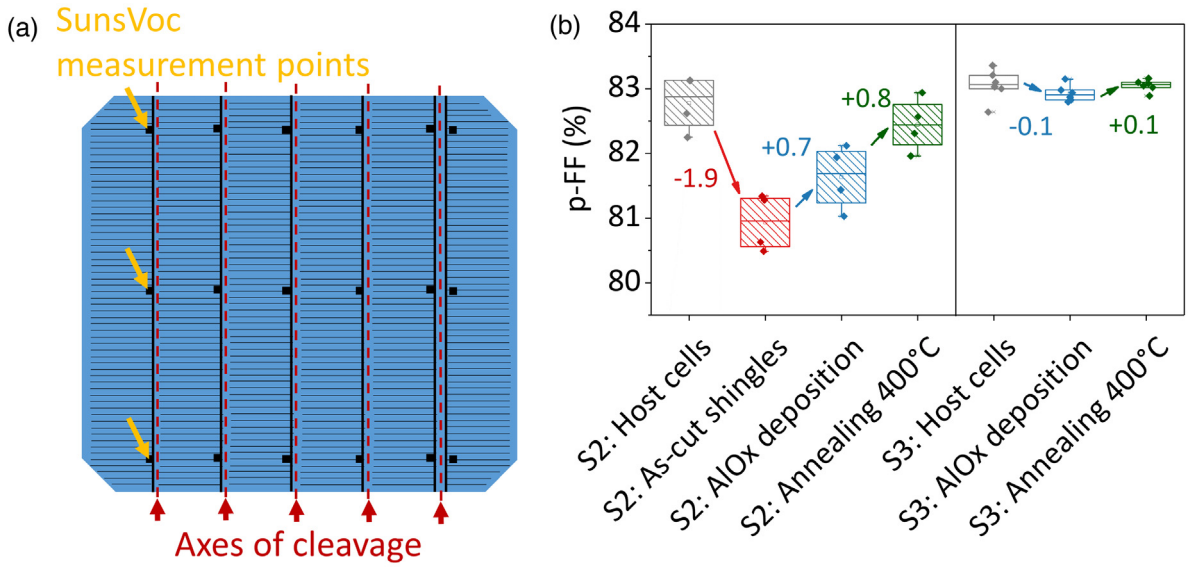

Fig. 4. (a) Schematic position of separation axes and example of contacting points on the left shingle during Suns V_{OC} measurements. (b) p-FF evolution for S2 and S3 groups.

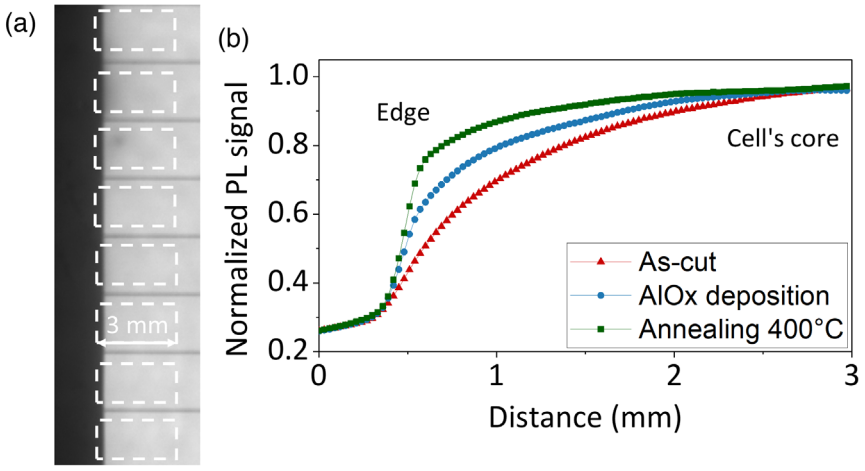

Fig. 5. (a) PL image of a passivated edge with the studied area annotated. (b) PL profile signal of an S2 shingle's edge along the passivation steps.

as Lohmüller et al. [26] have reported such p-FF improvements in their respective studies on bi-facial PERC and TOPCon solar cells, after similar AlO_x deposition process (i.e. thermal ALD). AlO_x is known to have high hydrogen concentrations, especially for low-temperature as-deposited (100 °C) AlO_x layer [14], which effectively decrease carrier's recombination by reducing the interface trap density. After the post-deposition thermal treatment, we report a further p-FF increase of about $0.8\%_{abs}$, bringing the overall increase to $1.5\%_{abs}$. Compared to the losses of the S2 group cells after cleave, the whole passivation sequence (AlO_x deposition and annealing step) allows an $79\%_{rel}$ p-FF loss recovery. Thus, the resulting p-FF loss for cleaved and passivated shingles compared to the host cells is only $0.3\%_{abs}$. For the S3 reference group, we observe little evolution: $0.1\%_{abs}$ approximate loss right after AlO_x deposition followed by a $0.1\%_{abs}$ increase after annealing. This observation indicates the effective edge passivation of the S2 shingle, as the whole treatment seems to rather have no significant effect on the non-cut M2 cell. However, in our case, we would have expected a greater impact from the 400 °C thermal treatment, as the passivation properties of the AlO_x after the subsequent high temperature-annealing step usually significantly exceed the as-dep passivation level [14]. The chemical passivation improvement after annealing is considered marginally compared to the large increase of the FEP [15,16].

Figure 5a shows the PL image of a passivated edge under 1 sun illumination, with the 1 mm × 3 mm areas from which the profile was extracted on ImageJ. Figure 5b displays the corresponding edge PL profiles for each step of the passivation protocol. We can see that both AlO_x deposition and annealing improve the PL signal at the vicinity of the edge. These results reflect a decrease in edge defect-related recombination and thus confirm the effective edge-passivation hypothesis previously made.

The IV parameters of the three sample groups are shown in Figure 6 and compared to those of their respective post-metallization host cells. We observe some difference between the three host cells groups, especially in V_{OC}. Those initial performance discrepancies are due to variability in the cell fabrication process. Although IV performances of the S2 samples after shingling and before passivation were not measured, we expect the losses induced by the cleavage to be similar for both groups. Indeed SunsV_{OC} results have shown similar losses in term of p-FF and V_{OC} (not shown) for S1 and S2 groups after cleavage.

Edge-related losses appear to be significantly lower for the S2 passivated shingles split in comparison with the S1 as-cut shingles split. Efficiency and FF mean losses are reduced at $0.4\%_{abs}$ and $0.4\%_{abs}$, respectively, while as-cut shingles feature $1.3\%_{abs}$ and $3.6\%_{abs}$ corresponding decreases. Moreover, the V_{OC} shows almost no variation for the S2 group in mean after cleave and passivation, while the value for as-cut S1 group drops of about 4.8 mV. This suggests that the good performances of passivated shingles are due to an effective reduction of the edge passivation.

However, we notice a slightly larger short-circuit current density (J_{sc}) loss for S2 than for S1 (0.5 versus 0.3 mA/cm^2). A part of this J_{SC} loss is also visible for the S3 cells after the AlO_x deposition and annealing steps but without the cleave, indicating that our edge passivation protocol may not yet be optimized concerning the optical properties of the devices. Indeed, we deposited the AlO_x layer not only at the edges, but also on the front side of the cells, which is expected to affect the optical characteristics of the device. In addition, a modification of the optical and/or electrical properties of the device caused by the thermal annealing cannot totally be ruled out [33,34].

Figure 7a presents a LBIC mapping of a shingle displaying the exploited areas. Profiles of a S2 passivated and a S3 unpassivated edge (now after mechanical cleaving) are presented in Figure 7b. We can notice a higher local current close to the edge for the passivated samples. This result further confirms the effective edge passivation interpretation previously presented. Furthermore, it supports the idea that the J_{sc} losses observed for S2 are not only edge-induced but more likely related to optical issues.

The observed passivation is considered to arise from a reduction in the recombination rate at the edge. This reduction is expected to result from both a good chemical passivation (Dit reduction via an interfacial SiO_x layer combined with the presence of hydrogen atoms [15]) and a strong field effect (due to the presence of negative fixed charges). It would be interesting to further investigate the respective contributions of the chemical and field effect passivations as well as considering other mechanisms that may contribute to the observed losses and recovery, such as effects related to the pn junctions (i.e. here the interface between the poly-Si collectors and the c-Si susbtrate) [31].

Despite those already satisfying results, further improvements are achievable. Methods to scale up the mechanical cleavage, here manually conducted and thus

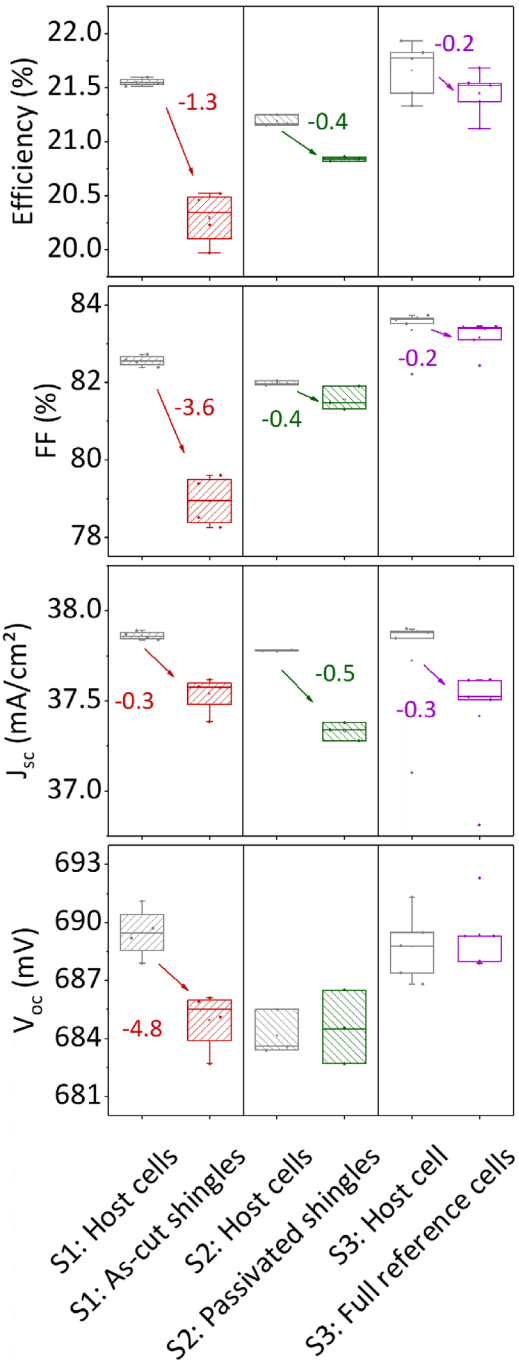

Fig. 6. IV measurement results for the three studied conditions compared to the corresponding unprocessed host cells. Absolute differences are annotated.

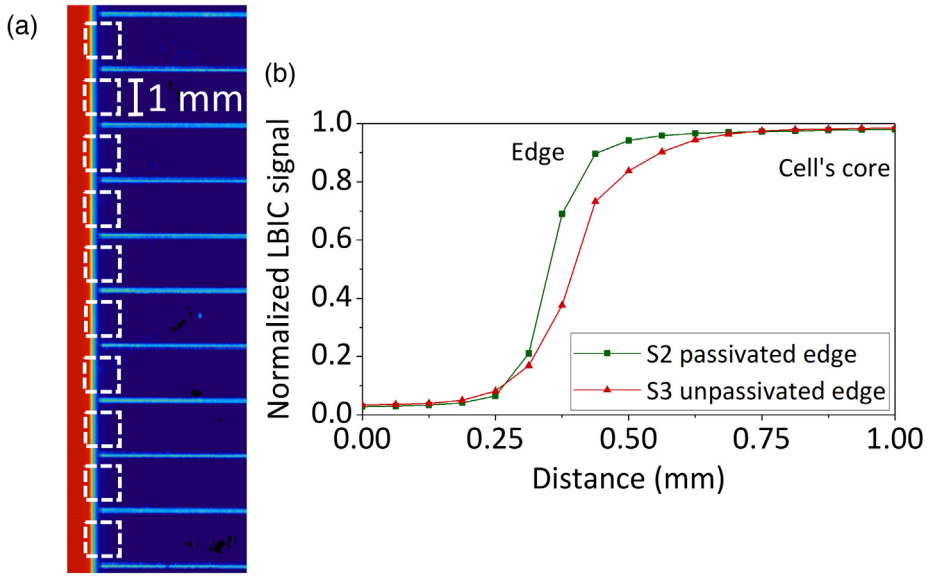

Fig. 7. (a) LBIC mapping (852 nm laser) with the studied areas annotated. (b) LBIC profiles of an S2 passivated and an S3 unpassivated edge. Both samples have an AlO_x layer on the front and the rear sides.

not suitable for industrialization, are currently under investigation. In addition, this could allow a standardization of the cleavage quality.

Regarding the optical matter, the 70 nm-thickness of the TCO layer was initially found to be optimal as anti-reflective layer in a case where no additional capping was present. Therefore, optimising both the AlO_x and TCO thicknesses, aiming a double anti-reflective capping, should result in better optical characteristics for the passivated devices. We believe this to be a solution to reduce the J_{SC} losses discussed above. Next studies should also involve optical simulations considering the triple participation of AlO_x, TCO and encapsulation layers at the module level.

Although shingle interconnection were successfully done for silicon heterojunction cells with a 15 nm AlO_x layer [35], the impact of the passivation protocol on the contacting quality and the reliability of the modules must be assessed in following studies.

4 Conclusion

The innovative combination of mechanical cleaving by the "*45° tilt squaring approach*" with thermally activated ALD AlO_x layers was successfully applied on advanced double-side poly-Si/SiO_x shingled solar cells. Although the presence of the AlO_x layer on the front side combined with a high temperature thermal treatment seems to slightly deteriorate the front side optical properties, as we witness current density losses for every sample groups, this edge passivation protocol led to significant performance improvements. We report a $79\%_{rel}$ recovery of cut-related p-FF losses. Passivated shingles show efficiency and FF values exceeding by $0.5\%_{abs}$ and $2.6\%_{abs}$, respectively, those of as-cut (i.e. non-passivated) shingles. In addition, the V_{OC} level was preserved for passivated shingles in comparison to their host cells, while unpassived shingles suffered from a 4.8mV loss after cleavage. LBIC analysis demonstrated the benefits of the developed edge passivation treatment on local current generation, and PL characterization highlighted the involvement of both AlO_x deposition and annealing steps on the edge passivation.

Authors would like to gratefully acknowledge the support of the European Union through the funded Horizon Europe research and innovation program IBC4EU under GA No. 101084259, and the French Environment and Management Agency (ADEME) for co-funding Franck Dhainaut's PhD.

Author contribution statement

Franck Dhainaut: Writing – review & editing, Methodology, Investigation. Raoul Dabadie: Characterization. Benoit Martel: Methodology, Review. Thibaut Desrues: Supervision, Resources, Investigation, Review. Mickaël Albaric: Supervision, Methodology, Investigation, Review. Olivier Palais: Supervision, Review. Sebastien Dubois: Review. Samuel Harrison: Methodology.

References

1. D.M. Fischer, ITRPV | ITRPV 2023 | PV CellTech, Berlin (2023)
2. N. Klasen et al., IEEE J. Photovolt. **12**, 546 (2022)
3. D. Tonini et al., Energy Procedia **150**, 36 (2018)
4. J. Zhao et al., IEEE Electron Device Lett. **18**, 48 (1997)
5. M. Mittag et al., in *Proceedings of the 2017 IEEE 44th Photovoltaic Specialist Conference (PVSC), Washington, DC, USA* (IEEE, 2017), pp. 1531–1536
6. S. Chowdhury et al., New Renew. Energy **16**, 1 (2020)
7. C. Hollemann et al., Progr. Photovolt. : Res. Appl. **27**, 950 (2019)

8. F. Gérenton et al., Sol. Energy Mater. Sol. Cells **204**, 110213 (2020)
9. A. Fell et al., IEEE J. Photovoltaics **8**, 428 (2018)
10. V. Giglia et al., in *Proceedings of the 37th European Photovoltaic Solar Energy Conference, France* (2020), pp. 282–285
11. K. Ruhle et al., IEEE J. Photovolt. **5**, 1067 (2015)
12. W. Li et al., Adv. Energy Sustain. Res. **2022**, 2200154 (2022)
13. M. Pawlik et al., Energy Procedia **60**, 85 (2014)
14. G. Dingemans et al., J. Appl. Phys. **111**, 093713 (2012)
15. S. Kühnhold-Pospischil et al., Appl. Phys. Lett. **109**, 061602 (2016)
16. R.S. Bonilla et al., Phys. Status Solidi A **214**, 1700293 (2017)
17. B. Hoex et al., J. Appl. Phys. **104**, 044903 (2008)
18. G. Dingemans et al., Electrochem. Solid-State Lett. **14**, H1 (2011)
19. G. Dingemans et al., Electrochem. Solid-State Lett. **13**, H76 (2010)
20. C. Barbos et al., Energy Procedia **77**, 558 (2015)
21. S. Bordihn et al., Energy Proc. **27**, 396 (2012)
22. B. Vermang et al., in *Proceedings of the 2011 37th IEEE Photovoltaic Specialists Conference, Seattle, WA, USA* (IEEE, 2011), pp. 1144-1149
23. H.B. Profijt et al., J. Vacuum Sci. Technol. **A 29**, 050801 (2011)
24. P. Baliozian et al., IEEE J. Photovolt. **10**, 390 (2020)
25. B. Martel et al., Sol. Energy Mater. Sol. Cells **250**, 112095 (2023)
26. E. Lohmüller et al., Progr. Photovolt. (2023), https://doi.org/10.1002/pip.3680
27. F. Feldmann et al., Sol. Energy Mater. Sol. Cells **120**, 270 (2014)
28. T. Desrues et al., in *Proceedings of the 2021 IEEE 48th Photovoltaic Specialists Conference (PVSC) Fort Lauderdale, FL, USA* (IEEE, 2021), pp. 1069–1072
29. J. Lelièvre et al., in *Proceedings of the 37th European Photovoltaic Solar Energy Conference, France* (2020), pp. 487–489
30. J. Wong et al., IEEE Trans. Electr. Devices **62**, 3750 (2015)
31. H. Stolzenburg et al., in *Proceedings of the 15th International Conference on Concentrator Photovoltaic Systems (CPV-15), Fes, Morocco*, (2019), 020017
32. L. Zhao et al., J. Eur. Ceram. Soc. **38**, 1038 (2018)
33. L. Tutsch et al., in *Proceeding of the 8th International Conference on Crystalline Silicon Photovoltaics, Lausanne, Switzerland* (2018), p. 040023
34. F. Meyer et al., Sol. Energy Mater. Sol. Cells **219**, 110815 (2021)
35. S. Harrison et al., in *Proceedings of the 8th World Conference on Photovoltaic Energy Conversion, Milan, Italy* (2022), pp. 55–58

Cite this article as: Franck Dhainaut, Raoul Dabadie, Benoit Martel, Thibaut Desrues, Mickaël Albaric, Olivier Palais, Sébastien Dubois, Samuel Harrison, Edge passivation of shingled poly-Si/SiO_x passivated contacts solar cells, EPJ Photovoltaics **14**, 22 (2023)